Parametric study of H-Darrieus vertical-axis turbines using CFD simulations

Rémi Gosselin,[1, a)] Guy Dumas,[1] and Matthieu Boudreau[1]

Laboratoire de Mécanique des Fluides Numérique

Département de Génie Mécanique

Université Laval

Québec, Québec G1V 0A6

Canada

The following article appeared in *Journal of Renewable and Sustainanble Energy, 8, 053301 (2016)* and may be found at:
http://dx.doi.org/10.1063/1.4963240

A parametric study of vertical axis turbines of the H-Darrieus type is conducted using state-of-the-art CFD and the k-ω SST RANS model in its unsteady form. Although most parameters have previously been investigated individually, the effect of solidity, number of blades, tip speed ratio, Reynolds number, fixed blade pitch angle and blade thickness on the aerodynamic efficiency of the turbine is evaluated using the same performance evaluation set-up in order to determine what would be the best aerodynamic configuration and operation parameter in a given application. The quantitative impact of 3D effects associated to the blade aspect ratio and the use of end-plates is also investigated. For high-Reynolds applications, optimal radius-based solidity is found to be around $\sigma = 0.2$, while higher solidities show a lower maximum efficiency than what was previously published using simpler streamtube based methods. In 3D, a small blade aspect ratio ($AR = 7$) leads to a relative efficiency drop of nearly 60% compared to the 2D prediction. Longer blades improve the 3D efficiency greatly. End-plates are found to have a positive effect on power extraction performances, as long as their size and thus their drag is limited.

Keywords: H-Darrieus; Vertical Axis; Wind turbine; Hydrokinetic turbine; uRANS; CFD; Dynamic stall

[a)]Electronic mail: remi.gosselin.2@ulaval.ca

NOMENCLATURE

α	Blade angle of attack, see Fig. 3
α_0	Blade pitch angle, see Fig. 3
β	Force angle, see Fig. 3
η	Turbine efficiency ($\eta \equiv \overline{C_P}$)
λ	Blade Tip Speed Ratio (TSR)
ν	Fluid kinetic viscosity
ω	Turbine angular velocity ($\omega = \frac{d\theta}{dt}$)
ρ	Fluid density
σ	Solidity based on turbine radius ($\sigma = Nc/R$)
θ	Azimuth angle
A	Swept area of the turbine ($2R \times H$ in the case of a H-Darrieus turbine)
AR	Blade Aspect Ratio $AR = H/c$
c	Blade chord length
C_P	Instantaneous power coefficient, ratio of power extracted to power available, see Eq. 1
$\overline{C_P}$	Cycle-averaged power coefficient, see Eq. 2
D	Drag force on a blade
F_N	Normal force on a blade
F_T	Tangential force on a blade
H	Turbine height
L	Lift force on a blade
M	Moment around the turbine axis of rotation
N	Number of blades
R	Turbine radius
Re	Reynolds number based on blade rotational speed ($Re = R\omega c/\nu$)
U_∞	Free stream velocity

I. INTRODUCTION

The vertical-axis turbine (VAT; wind turbine: VAWT; or hydrokinetic turbine: VAHT) concept was originally proposed by George Darrieus in the 30s[1], but has not been developed since then as much as horizontal-axis turbines (HATs), despite many interesting characteristics.

The main advantage of VATs compared to HATs is that they are axisymmetric, meaning that an orientation mechanism is not needed whatever the upstream flow direction. On the other hand, vibrations induced by the non-constant forces on the blades lead to a real mechanical challenge and one of the main reasons why this design principle is not as popular as it could be among current turbine manufacturers.

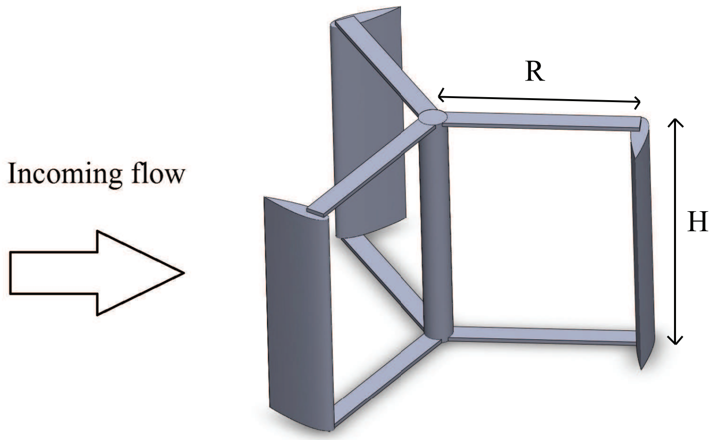

FIG. 1. Global view of a vertical axis turbine.

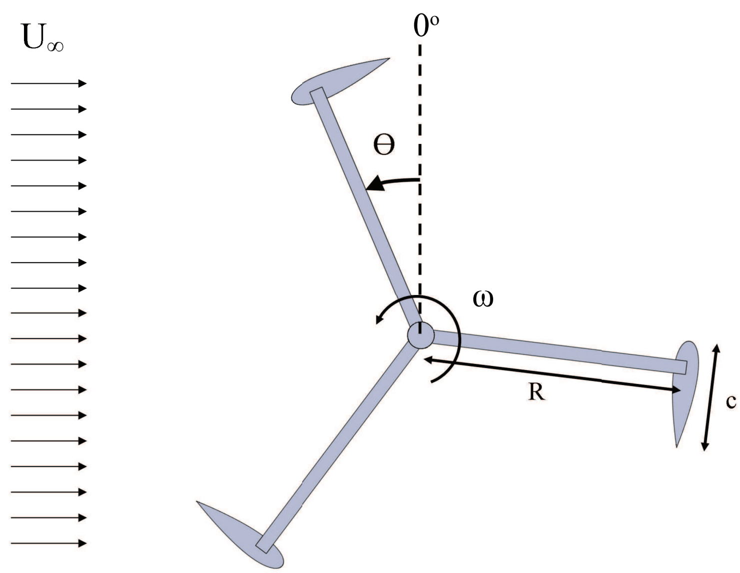

FIG. 2. Different geometric parameters and azimuth angle (θ) of a Darrieus turbine.

The power extraction performance of a VAT is governed by the following 2D parameters:

- Blade profile and chord (c)
- Number of blades: N
- Solidity based on the turbine radius: $\sigma = \frac{Nc}{R}$
- Tip speed ratio (TSR): $\lambda = \frac{R\omega}{U_\infty}$
- Reynolds number based on blade rotational speed: $Re = \frac{R\omega c}{\nu}$.

There are also various 3D parameters that influence the aerodynamic efficiency, among which we find:

- Blade aspect ratio: $AR = \frac{H}{c}$
- Blade configuration (straight blade, helix, "eggbeater", canted...)
- Presence and shape of end-plates and blade connecting arms.

The instantaneous power coefficient C_P is defined as the ratio of the power extracted to the power available, the power extracted being equal to the torque generated around the shaft $M(\theta)$ multiplied by the turbine angular velocity ω:

$$C_P(\theta) = \frac{M(\theta)\ \omega}{\frac{1}{2}\ \rho\ U_\infty^3\ A} \quad , \tag{1}$$

where A is the swept frontal area ($2R \times H$ in the case of a H-Darrieus turbine).

The aerodynamic efficiency of the turbine $\overline{C_P}$ is given by the average power coefficient C_P over one revolution:

$$\eta \equiv \overline{C_P} = \frac{1}{2\pi} \int_0^{2\pi} C_p(\theta)\ d\theta \quad . \tag{2}$$

Different geometric parameters, force components and important geometric angles are also defined in Figs. 2 and 3.

Simulation of such turbines over a wide range of TSR is particularly challenging because the aerodynamics strongly depends on the turbine rotational speed. High TSRs imply low angles-of-attack and small variations, but strong wake interferences, even in the upstream phase, whereas low TSRs cause the blades to undergo large variations of their angles of attack and effective flow velocities, eventually leading to dynamic stall.

Following the energy crisis in 1974, the U.S. government decided to fund a vast research program on alternative energy sources, including wind turbines. A team at the Sandia National Labs in Albuquerque, New Mexico, conducted a vast experimental study of the original Darrieus concept, both on wind tunnel models and full-scale turbines. One of their full-size turbines reached nearly 40% efficiency[2], which is close to a typical large HAWT (45%)[3].

Early numerical models developed in the 80s by Templin at the National Research Council Canada[4], Strickland and Mays at the Sandia National Laboratories[5,6] and other smaller teams[7,8], later improved by Paraschivoiu in the 90s and 2000s[9], were based on double or multiple streamtubes to attempt to predict the efficiency of Darrieus turbines. While they provide a good prediction of

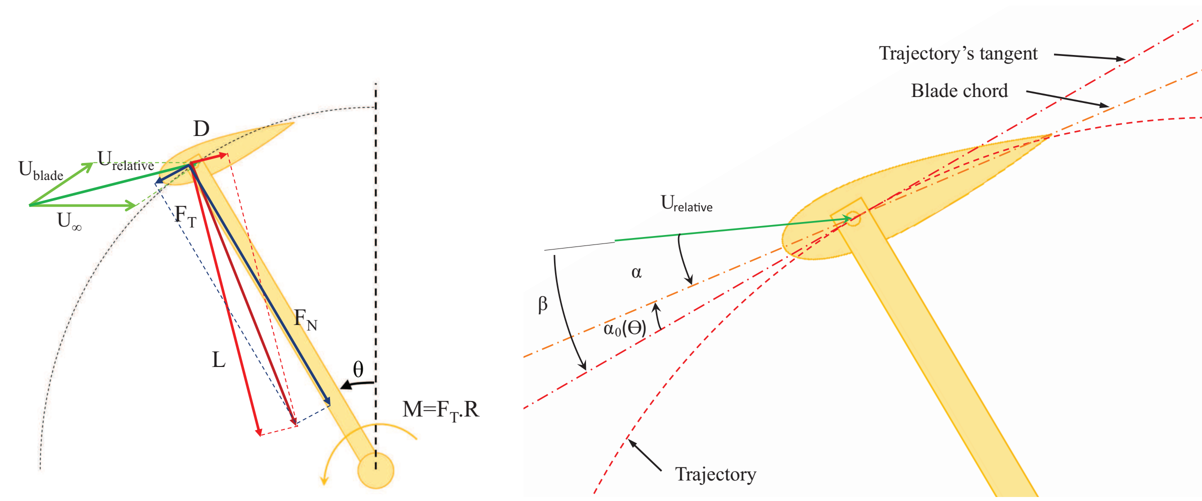

a. Detail of torque generation (M) from a blade in a vertical axis turbine.

b. Details of the pitch angle (α_0), angle of attack (α) and force angle (β) of a turbine blade. Angles are defined counter-clockwise.

FIG. 3. Detail of forces and various angles on a turbine blade.

the performances observed at high TSRs, they tend to over-estimate the efficiency level at lower tip speed ratios. This has been widely confirmed by recent wind tunnel experiments on small-scale wind turbines by Howell et al.[10,11] and Armstrong et al.[12], whose high-solidities turbines (around $\sigma = 0.5$ and above) could not reach the efficiency value above 40% predicted by these models. Water channel experiments performed by MAVI Innovations[13] and later published by Li and Calisal[14] also confirmed this lack of efficiency for medium to high solidities turbines. All these small scale experiments, with a certain degree of flow confinement, show a measured efficiency between 25% and 30%.

More up-to-date CFD simulations have been carried out, often in parallel with small-scale experiments, for example by Ferreira et al.[15], who explored the different turbulence models available, along with space and time discretization, while using PIV to validate their choices. They tested time discretization up to 0.25° per time-step (1440 time-steps/cycle), and two various grid refinements. However, their numerical results showed no numerical independence, demonstrating the need for a proper numerical approach to the problem. Another example is the simulations presented by Howell and al.[10], using k-ϵ for turbulence modeling, albeit with a modified wall function to account for the low Reynolds numbers ($Re = 30000$, $Re = 34000$ and $Re = 39000$) associated with the small-scale turbine. Their results show a reasonable agreement with the experimental results, and a decreasing gap between the two methods when the Reynolds number increases. Finally, Castelli et al.[16] recently proposed a new performance prediction model based on CFD, also based on validation from a small-scale turbine. Their goal was to reduce the computational cost of the method by combining CFD and the simpler blade element method to determine the power curve. The proposed model tend to show a good agreement with their wind tunnel data, but the choice of turbulent model (k-ϵ with modified wall function) and the time discretization used (360 times-steps per cycle), while giving acceptable results in a low Reynolds confined configuration, could create problems in more challenging cases with higher Reynolds numbers and no flow confinement. All these results however are only validated with small Reynolds number turbines, in partially confined wind tunnels, and while they show the potential of efficiency prediction using a CFD approach, they do not give significant results and are not used as a tool to refine the design of full-size vertical axis turbines.

Finally, the effect of a majority of the parameters studied here has already been explored in previous studies. For example, Templin[4] published performance predictions with varying solidities as early as 1974, based on multiple streamtubes modelisation. A later publication by Marini et al.[17] focused more on the effect of the Reynolds number on $\sigma = 0.4$ and $\sigma = 0.15$ turbines, still using both a momentum and a free wake vortex model. The efficiencies observed matched Templin's observations, with a $\sigma = 0.4$ turbine have a predicted efficiency equal to that of a $\sigma = 0.15$ turbine, contrary to full-scale, unconfined observations by the Sandia National Laboratories. Rawlings[18] then Li and Calisal[14] also used a vortex method to evaluate the effect of the blade aspect ratio, and determined that blades with $AR = 72$ reach 95% of the efficiency of their 2D counterpart. Recent publications by Tjiu et al.[19,20] do a good review of the effect of various 3D configurations, showing the unexploited potential of vertical axis turbines compared to horizontal axis turbines. A coupled fluid-structure approach, combining a discrete vortex method for the fluid and a finite element analysis for the blade was explored by Li et al.[21] to study the relationship between the turbine aspect ratio and the deflection of the blades. While the fluid modelisation is simpler than full Navier-Stokes solvers, the results presented give a good idea of how far designers can go in terms of turbine aspect ratio.

The present paper seeks to refresh and precise the current knowledge of the effect of each parameter on the aerodynamic efficiency of the turbine through carefully conducted, high Reynolds number, 2D and 3D CFD unconfined simulations, giving efficiency values closer to the reality than what was predicted by earlier models, especially when it comes to the solidity effect. By having a fixed modelisation approach, the effect of each parameter and the associated predicted efficiency values can be compared from one to another. We also aim to develop a better understanding of its basic aerodynamics and to estimate the 3D finite-span effects with complete 3D low AR CFD simulations in order to confirm Li and Calisal results, and test if the presence of end-plates could improve the global efficiency of the turbine, despite the large sensitivity of the Darrieus principle to drag.

II. SIMULATION METHOD

A. Numerics

In the present study, the numerical simulations are performed with the commercial finite-volume code ANSYS FLUENT[22]. The simulations are conducted using the SIMPLE (Semi-Implicit Method for Pressure-Linked Equations) velocity-pressure coupling algorithm. Second order schemes are used for pressure, momentum, turbulent kinetic energy (k) and specific dissipation rate (ω) formulations. A second order implicit scheme is used for time integration. Absolute convergence criteria are set to 10^{-5} for each variable (continuity, velocity components, turbulence kinetic energy and specific dissipation rate).

B. Turbulence modeling

Several turbulence models exist, among which Spalart-Allmaras, k-ϵ and k-ω are the most commonly used for engineering applications. The k-ω SST (*Shear Stress Transport*) model is a combination of the last two: k-ω model is used near the walls whereas the far field is resolved using k-ϵ. While k-ϵ uses a wall function to resolve the boundary layer, the other two models solve the Reynolds-averaged Navier Stokes equations up to the wall. This means the mesh density near the walls has to be adapted in order to be able to capture all of the viscous sublayer of the boundary layer. A commonly used criterion is the y^+ factor, which needs to be of order 1 for a model without wall function, and around 40 for a model using one (the precise value depends on the wall function used).

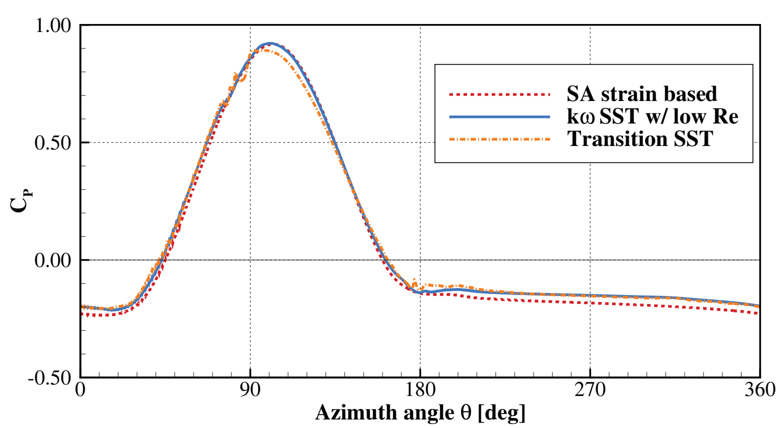

FIG. 4. Turbulence modelling behaviour at high TSR ($\lambda = 4.25$) for a turbine with $\sigma = 0.5486$ and 3 blades (C_P illustrated here is for one blade only) operating past the peak efficiency occurring at $\lambda \approx 3.00$, with $Re = 2.55 \times 10^5$.

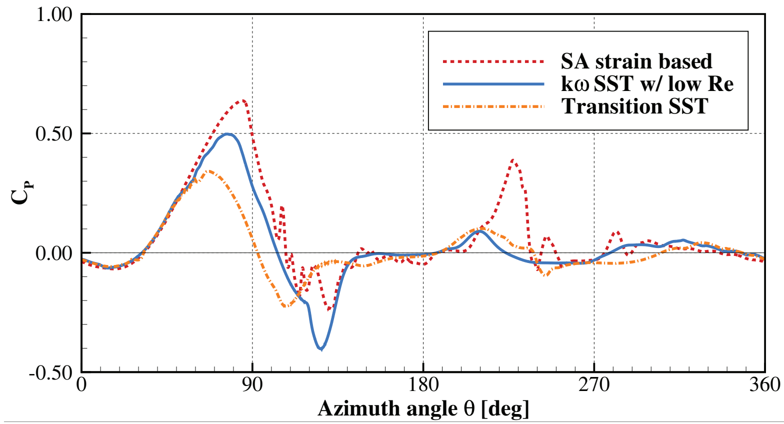

FIG. 5. Turbulence modelling behaviour of the same turbine at low TSR ($\lambda = 2.55$), below peak efficiency, and $Re = 1.5 \times 10^5$.

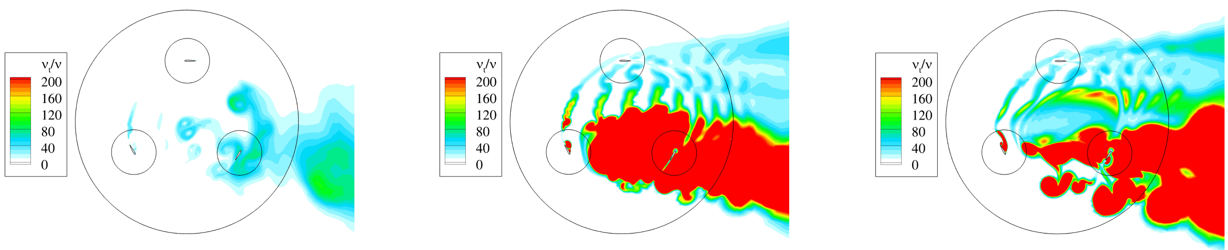

a. Spalart-Allmaras.

b. k-ω SST with low Reynolds correction.

c. Transition SST.

FIG. 6. Comparison of the contours of turbulent viscosity ratio at $\lambda = 2.55$ for different turbulence models.

In most cases where the boundary layer stays attached to the body, k-ϵ yields results similar to the other models while using a coarser mesh near the walls, which reduces the time needed to complete the calculations. However, in cases with boundary layer separations and dynamic stalls such as one observes in low TSRs cases, a wall function isn't appropriate to capture all the physical phenomena taking place in this important part of the flow field, and results are often off from reality[15,16,23].

Resolving the Navier-Stokes equations up to the walls is costly mesh-wise, but this kind of turbulence modelling has led to better agreement with experimental data, especially in oscillating airfoils and dynamic stall problems, or more generally in cases with boundary layer separations[23].

A brief comparison of three popular turbulence models, Spalart-Allmaras with modified production term (strain-based[24,25]), k-ω SST with low Reynolds corrections (damping of the turbulent viscosity[22]) and Transition SST has been made on the same turbine case ($\sigma = 0.5486$, 3 blades, NACA0012 profile). Resulting instantaneous power coefficients for each model are shown in Figs. 4 and 5. The first comparison is made at high TSR (4.25), for which the theoretical angles of attack (α) vary moderately (from $-14°$ to $14°$). The second one is made at low TSR (2.55), implying a high theoretical variation of α (from $-24°$ to $24°$) and consequently dynamic stall. As expected, the behaviour of the different models is quite similar in the high tip speed ratio case (Fig. 4), while results in the low tip speed ratio example (Fig. 5) vary significantly from one model to the other.

The main factor explaining these differences is the generation of turbulent viscosity, as illustrated in Fig. 6. The SA strain-based model generates around 10 times less turbulent viscosity than k-ω SST or Transition SST, resulting in a more chaotic flow field inside the turbine, and no statistical convergence of the instantaneous torque from cycle to cycle. It does not necessarily mean that the simulation is not representative of the reality, but from an engineering standpoint where one wants to compare a lot of different configurations and have an idea of the ideal parametric configuration, it is important to use a model that gives consistent results while being reasonably cheap to run. The simulation of a great number of turbine cycles is necessary in order to average the power output with this turbulence model. The Transition SST model gives similar results to k-ω SST in terms of cycle-averaged torque, but is less robust in some of the configurations tested. In the end, considering all its advantages in terms of dynamic stall representation and its relative low cost to run a full simulation, the k-ω SST model has been chosen to carry out the present parametric study.

C. Mesh and calculation strategy

The mesh is a critical part of a CFD simulation for engineering purposes. It has to be light enough so that the calculation is affordable, but also fine enough so that each important physical phenomena is well captured and simulated. The particular conditions observed in vertical axis turbines require high mesh densities not only at the blades but also inside the rotor to avoid damping the wakes of the blade for the downstream part of the cycle, as demonstrated by Zadeh et al.[26].

The idea here is to have a mesh that can be adapted to various configurations. Mesh interfaces (Fig. 7) are used between the calculation domain and the rotating turbine, and also between the "rotor" and the smaller blade area(s). The mesh zones that include the blades are identical between all the simulations in this work, ensuring that the boundary layer behaviour is similar between the various cases. The different mesh zones used for the present simulations are illustrated in Fig. 7 while various mesh details are shown in Fig. 8.

Unless otherwise specified (e.g., low rotational speed validation using Armstrong results[12]), the exterior domain in 2D is a square whose side is 1500 chord length. This has been checked to ensure that there is negligible blockage effect on the turbine.

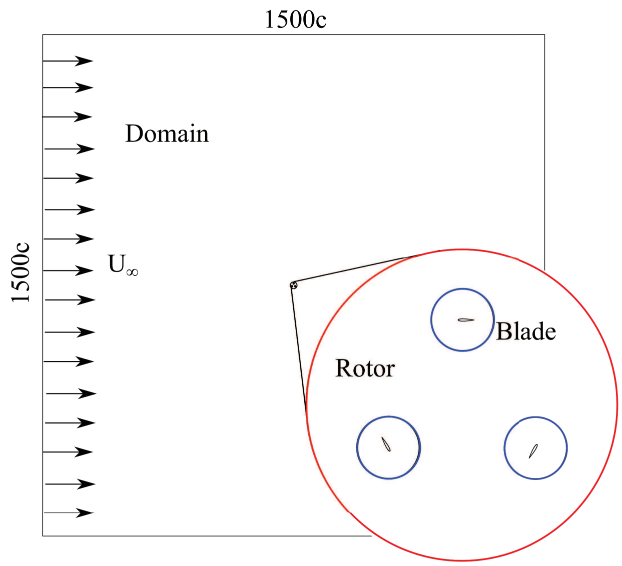

FIG. 7. Identification of the different mesh zones. The diameter of the rotor zone varies with the turbine radius. Red and blue lines are general mesh interfaces, allowing dynamic pitch motion.

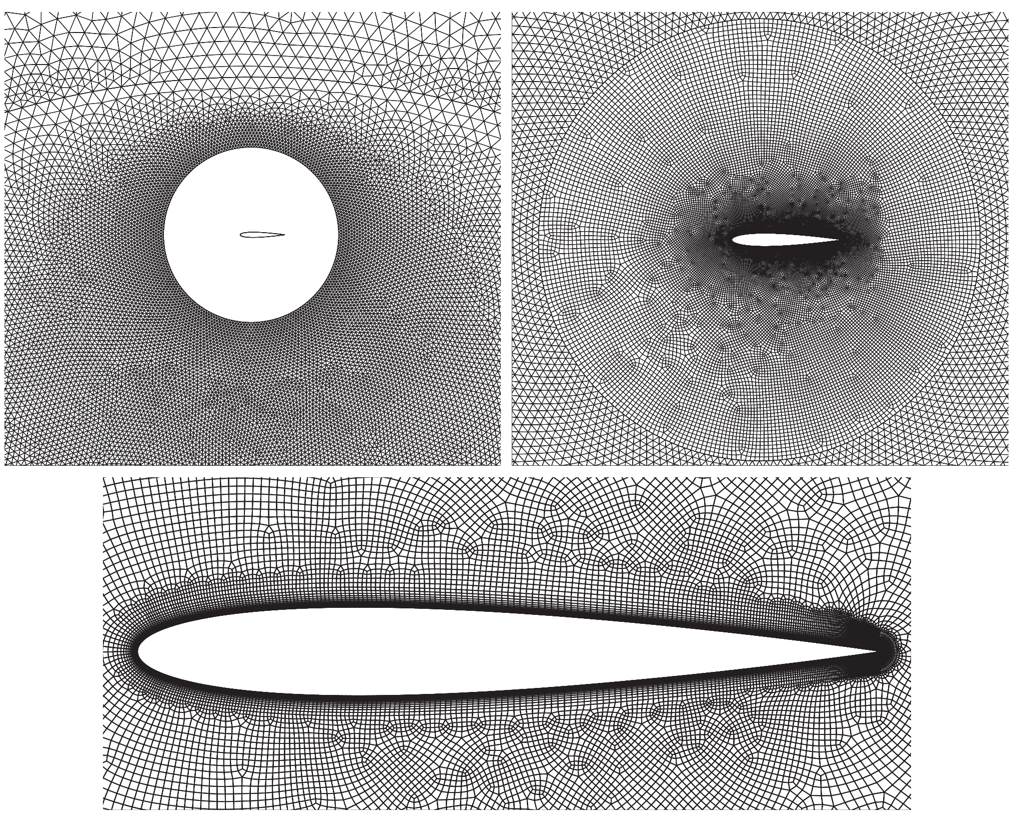

FIG. 8. Various details of the mesh.

Boundary conditions consist in two symmetry planes (top and bottom), a uniform mean pressure on the outlet boundary, and a uniform velocity on the inlet boundary with magnitude U_∞. The flow is quiet and clean at the inlet boundary with 0.1% turbulent intensity and $0.001c$ turbulent length scale, yielding $\nu_t/\nu \approx 0.05$.

A y^+ value of order 1 is sought at the blades in order to properly capture the boundary layer in non-separated conditions. The worst case scenario (high TSR, hence high Reynolds number and thin boundary layers) was used to determine the boundary layer thickness and thus the required cell's scaling. This implies that maximum y^+ is around 1 in high TSRs cases ($\lambda = 7$ and above) and smaller than 1 in lower rotational speed cases.

The number of nodes on each blade section is 360, but low TSR results have shown that it was not enough in deep-stall cases, probably due to difficulties in the prediction of the boundary layer separation position and in the resolution of the separation bubble. Finer meshes were tested in such conditions, with a lot more points (up to 700) on the blade section and finer boundary layer meshes, but no rigorous mesh-independence has formally been obtained as was the case for larger TSRs. Mesh sizes and typical calculation times associated with these meshes are shown in Table I.

A 3D mesh is also created based on an extrusion of the 2D mesh. Half the blade span is meshed in 3D and a symmetry boundary condition is imposed on the mid-plane. The spanwise discretization is uniform in the central part of the blade, close to the symmetry plane, while the last $0.5c$ length from the wingtip is refined. A first mesh was tested with 13 spanwise nodes per chord length on the central part, and a refinement close to the tip/end-plate with a y^+ value of 2. A second, coarser mesh, was tested with 7 spanwise nodes per chord length in the central part and $y^+ = 7$ at the wing tip, and showed no noticeable differences in the results along the cycle.

TABLE I. Comparison of the 2D mesh sizes tested and size of the 3D mesh used.

Mesh	Blade nodes	Total elements	Typical calculation time
2D	360	≈ 150000	2 days for 10 turbine cycles (8 CPUs)
3D	360	7 to 20 millions	30 to 90 days for 10 turbine cycles (64 CPUs)

Time step is expressed here on a per cycle basis. A quick comparison showed that around 1000 time steps per cycle were sufficient in most cases, but in particular instances needed up to 5000 to reach result independence. For this reason, this conservative value is used in all 2D simulations in order to avoid undesired effects on the flow field. For the 3D experiments (focused on high efficiency cases, with tip speed ratios higher than the optimum value, hence with no massive stall on the blades), we use the 1000 time steps per cycle value after verifying the results convergence with a 2500 time steps per cycle simulation. Other research groups have used much coarser time steps (e.g., around 360 time steps per cycle[16]), but our calculations showed that at such low values, result independence is not achieved with the present modelling approach.

A minimum number of rotations is necessary to ensure that a repeatable power extraction cycle is achieved, but this number is case-dependant and must be assessed for each simulation by comparing the C_P signal cycle to cycle. For example, high speed, unstalled case ($\lambda = 6.38$) of a low solidity ($\sigma = 0.1819$) three-blade turbine needs around 10 complete turbine cycles to reach cycle-averaged torque convergence. Other low speed cases need in excess of 20 turbine rotations to reach it. In all simulations presented here, cycle-averaged convergence was reached before accumulating data and statistics.

D. Model validation

1. High TSR, low solidity

High tip speed ratios ($\lambda = 4$ to 6) are the least challenging cases to simulate because the blades never actually reach too large effective angles of attack, hence never encounter stall. Since k-ω SST was developed for aeronautic applications, the results are expected to be satisfactory. However, good and reliable data on test turbines operating in this range of TSR are rare. The solidity needs to be low (σ from 0.1 to 0.2) to present a performance peak around $\lambda = 5$. This means high ratio of turbine radius to blade chord. The best example of such a turbine is the 5m Sandia

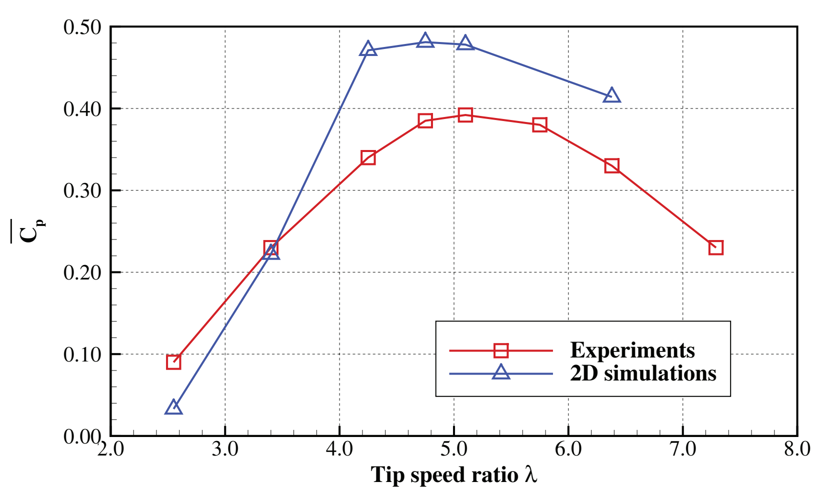

FIG. 9. Comparison of the experimental results for the Sandia 5m turbine, and 2D simulations of a three-blade, $\sigma = 0.1829$ turbine.

test turbine[2], which has 3 blades and mid-height solidity of $\sigma = 0.1829$, but has the shape of the original Darrieus, i.e., the "egg-beater" shape.

It has been shown that around the peak efficiency, most of the power is extracted in the central, almost straight-blade, area. In fact, most of original Darrieus turbines used three-part blades, with only the center, high local radius part, being profiled, the extremities only serving the role of connecting arms. The Sandia 5m turbine, however, used fully profiled blades. Because of that, a 2D simulation should give good results around the peak efficiency. At lower speeds, the power extraction is more evenly distributed along the turbine height, with upper and lower parts of the turbine having higher local solidities, hence being more efficient at these lower TSRs.

Results are presented in Fig. 9. As expected, the optimal tip speed ratio is relatively well represented. However, at lowers TSRs, the efficiency predicted by the 2D numerical simulation drops faster than the experimental data, due to the "egg-beater" shape of the turbine. The gap between experiments and 2D simulations is primarily the result of 3D effects, and a 20% difference, measured here around the peak, is not inconsiderate, as discussed in section III C 1.

2. *Low TSR, high solidity*

Low tip speed ratios ($\lambda = 1$ to 3) are far more difficult to simulate because of the high instantaneous angles of attack reached by the blades (see Eq. 3 and Fig. 13), combined with highly varying relative flow velocities. This leads to boundary layer separation and occurrence of dynamic stall in parts of the blade cycle for such cases.

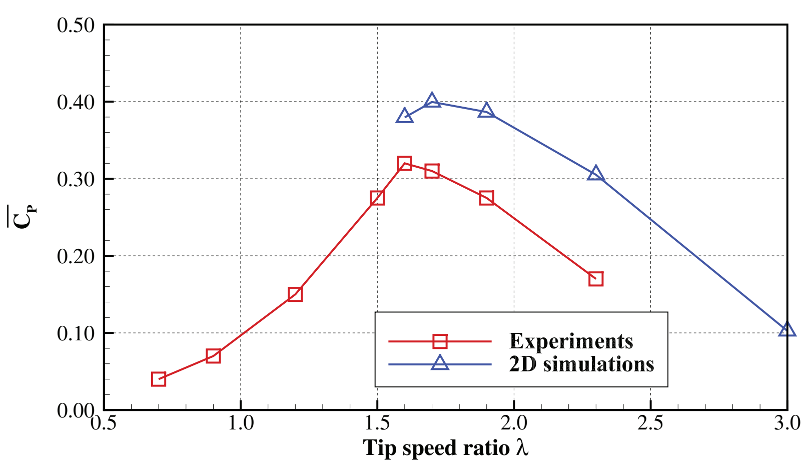

FIG. 10. Comparison of the experimental results and 2D simulations of a three-blade turbine, in the $-6°$ fixed pitch configuration with $\sigma = 0.915$.

Turbines operating in this range of TSR perform better with higher solidity (typically around 0.5), either by an increased number of blades or a reduced turbine radius. Examples of such turbines are more common in the literature as they are easier to manufacture and fit more easily in a wind tunnel or a water channel.

In this article, the simulations are compared to wind tunnel experiments by Armstrong et al.[12] whose straight-blades turbine has a solidity $\sigma = 0.915$ and a peak efficiency $\overline{C_P} = 0.27$ at $\lambda = 1.6$ and $Re = 5.0 \times 10^5$. It was tested at the University of Waterloo Live Fire Research Facility, whose dimensions and characteristics are described by Devaud et al.[27]. Our numerical domain size and boundary conditions have been modified for this particular case to match the experimental rig, albeit only in 2D.

They also provided results[12] with various pitch angles ($3°$, $0°$, $-3°$, $-6°$, $-9°$ and $-12°$) that can be used to further validate the model, with $-6°$ being the optimal configuration in this case.

Results of the simulations are presented in Fig. 10. Again, conditions for peak efficiency are well predicted despite the overestimation of the 2D simulations. Low TSRs, before the optimal value of $\lambda = 1.6$ were not simulated here, except for the $\lambda = 0.70$ case, which gave a cycle-averaged efficiency $\overline{C_P} = 0.02$, lower than what is observed on the test turbine. Low speed simulations of other configurations of this turbine (with no pitch angle α_0, see Fig. 3) showed the same behaviour as in the Sandia 5m simulation (Fig. 9), with the experimental curve being slightly higher than the simulation one.

Further discussion on the effect of the pitch angle α_0 is presented in the next section. The important thing to note here is that the model has a good behaviour past the optimal TSR, with an almost constant relative gap between the 2D simulations and 3D experimental results. This difference is mainly due to the various 3D effects present in the laboratory and also due to the particular shape of the "wind tunnel" used, with a ceiling high above the testing plane, and ground proximity.

E. Modelling limitations

Deep wing stall is always a challenge in CFD, so it's not unexpected that the simulations give poor matching of experimental data in theses cases, with lower efficiencies than what is observed in real turbines. On the other hand, they tend to give quite good estimations of the TSR where peak efficiency is obtained, and higher TSRs behaviour is in accordance with the experimental results.

The differences between 2D simulation predictions and real, 3D turbine performances are the result of 3D effects[14]. It depends on several factors, including the turbine shape and its surroundings, so it is complex and risky to extrapolate an efficiency value for a particular real turbine based solely on 2D results. However, the qualitative impact of varying 2D parameters should be well modelled and quite representative of the real 3D physics.

III. RESULTS AND DISCUSSION

A. Flow topology within the turbine

The power-extraction performance of each blade within a VAT is strongly linked to the effective flow conditions seen by the rotating blades. These effective conditions are characterized by the instantaneous effective velocity (magnitude and direction) and the instantaneous angle of attack. A reliable description of the actual flow around each blade is important when seeking methods to improve the global efficiency through the control of instantaneous blade angle.

1. Velocity magnitude and direction

The easiest assumption that can be made about the flow field across a VAT is to consider it uniform and equal to U_∞. This assumption is however too simplistic. Indeed, a turbine blade makes 2 passes in the same streamtube every machine rotation. In the first one, it extracts energy, thus reducing the kinetic energy available downstream by reducing the velocity magnitude. This is represented in Fig. 11.

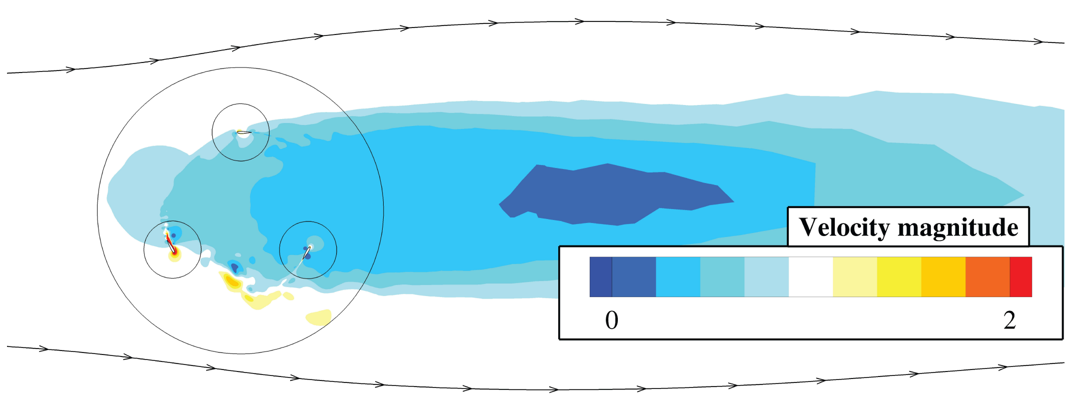

FIG. 11. Velocity magnitude contours and streamtube for a three-blade turbine with $\sigma = 0.5486$ and $\lambda = 2.75$. U_∞ is equal to 1 m/s.

This reduction in velocity, associated with the extraction of energy, also implies that the stream-tube expands while flowing through the turbine. This creates transverse velocities, also affecting the angles of attack, even in the upstream phase.

Another important point is that the flow velocity reduction is not symmetrical, as shown in Fig. 12. A drop in velocity magnitude is only observed downstream where the blade actually extracts energy, meaning that when it stalls, no significant drop in magnitude is noticeable downstream. If the TSR increases, the angles of attack drop, reducing stall, while the average relative velocity increases. It means that the turbine extracts more power during the first pass, eventually creating a low velocity area about the size of the turbine when no stall is observed. This decrease in available energy lowers the lift forces on the second pass, but also decreases the drag.

In the end, the best configurations are often those that extract most energy on the first 180° of the cycle (see the difference between Figs. 4 and 5 for example), with the second part creating considerably lower efforts on the blades due to the low local velocities and angles of attack.

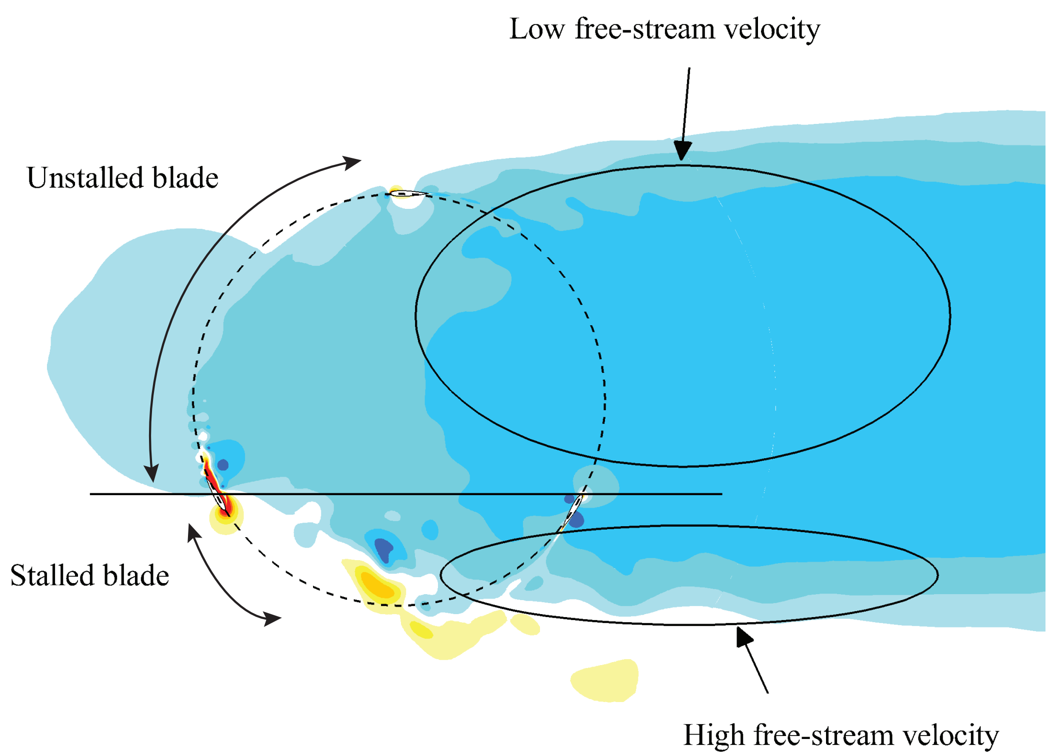

FIG. 12. Detail of the unstalled and stalled part of the cycle, linked to the velocity magnitude downstream.

2. Angle of attack: theory versus simulations

The instantaneous angle of attack can be estimated with Eq. 3, under the assumption of a uniform free stream velocity in the axial direction:

$$\alpha[rad] = \arctan\left(\frac{\sin(\theta)}{\lambda + \cos(\theta)}\right) \quad . \tag{3}$$

An example of these estimated angles of attack refered to here as "theoretical", for different TSRs is given in Fig. 13, which shows that the blades of a turbine operating at low tip speed ratios encounter much higher angles of attack than a turbine operating at high tip speed ratios. In the $\lambda = 5.10$ case, the theoretical angle of attack is never higher than the static stall angle for the profiles tested here ($\alpha_{stall} \approx 13°$).

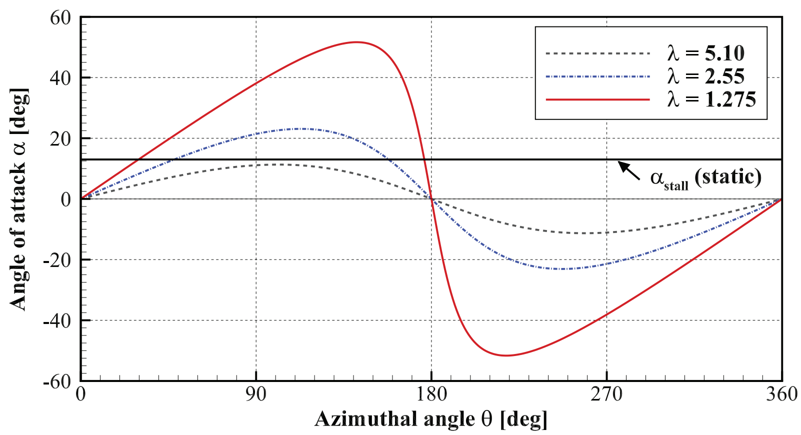

FIG. 13. Theoretical instantaneous angle of attack in a Darrieus turbine for different tip speed ratios (λ).

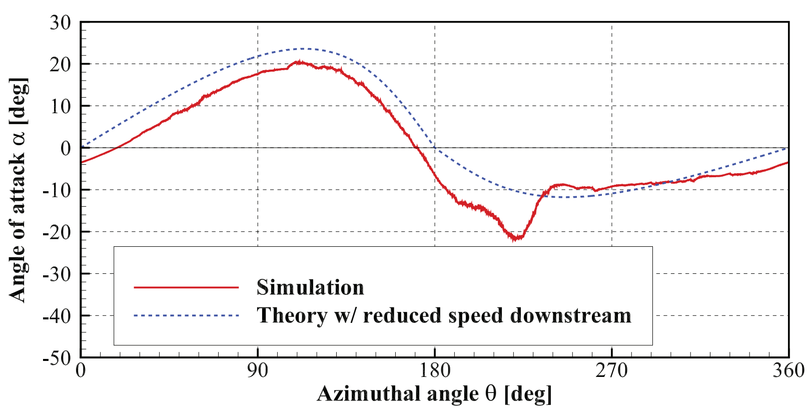

FIG. 14. Comparison between corrected theoretical angle of attack (flow velocity divided by 2 in the downstream part), and measured angle of attack from CFD simulation. Tip speed ratio is $\lambda = 2.5$ with a three-blade $\sigma = 0.5486$ turbine.

In cases where the turbine extracts significant power from the flow, we improved accuracy by using a reduced flow speed for the return part of the cycle, for example $0.5 \times U_\infty$. This would actually divide the angle of attack by 2 in the downstream part of the cycle, as shown by the theory curve of Fig. 14. This correcting factor would depend of course on the amount of power extracted in the first, upstream pass.

Even though the angle of attack is formally defined as the angle between the airfoil chord and the flow direction far from the foil, it is possible to extract a "local" angle of attack from the CFD data, by considering the average flow direction and magnitude along the blade path at a virtual point located two chord length ahead of the blade on its trajectory. This method gives a good estimate of what the real effective angle of attack of the blade is as shown in Fig. 14 which corresponds to a low-speed case where stall and boundary layer separation occur. Detailed explanations of this method are presented in Ref [28][28]. Significant differences between theory and simulations in the 180° to 240° range are thus expected, and are due to the turbulence and the surplus in kinetic energy available (creating more drag) linked to the stalling blade in the upstream phase.

The other difference between theory and simulation in Fig. 14 is the more or less constant gap in the upstream part of the cycle. This is due to the global blockage effect induced by the turbine, that affects the flow upstream of it. The relative velocity seen by the blade is not exactly U_∞, but a slightly lower velocity with a slight angle, since some of the flow tends to go around the turbine and not through it. More energy extracted means greater blockage.

B. 2D parametric study

1. Effect of the solidity

Earlier models based on multiple streamtubes were used in the 80s to make a global parametric study, especially on the effect of solidity σ[4,6,29]. These models predict $\overline{C_P}_{max} \geq 0.4$ even for high solidity turbines ($\sigma \approx 0.5$). However, such good performances have not been achieved experimentally for turbines with high solidities[10,11,14,30].

Figure 15 compares the results of the present 2D simulations of three-blade turbines with various solidities. The main difference with older theoretical models appears in the lower TSR region, where angles of attack are large enough to actually cause dynamic stall, which reduces power extraction. The maximum efficiency decreases when solidity increases, which is in accordance with experimental observations. Those are 2D results which implies that actual quantitative values are expected to be less in 3D. Three-dimensional simulations are needed to evaluate this impact, and are discussed in section III C.

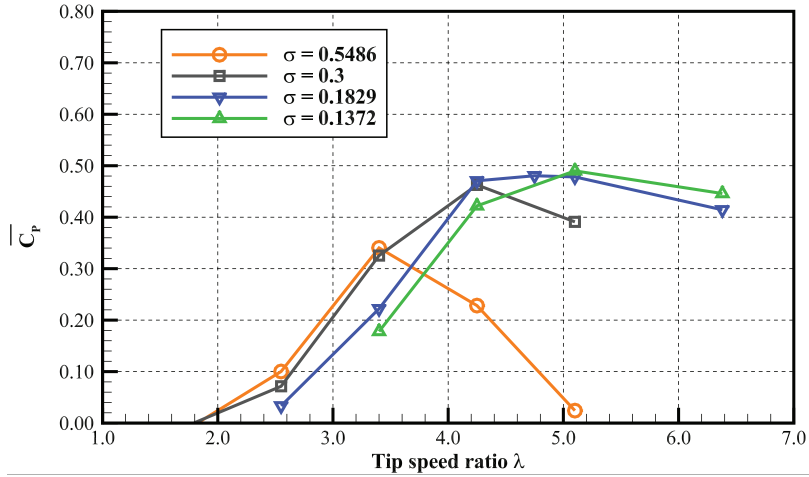

FIG. 15. Present CFD simulation of three-blade turbines with different solidities σ.

2. *Effect of the number of blades*

The number of blades has an effect on the global torque. More blades leads to a smoother torque on the shaft (less fluctuations). However, increasing the number of blades means increasing the number of connecting shafts, hence increasing the turbine drag. It also implies that for the same radius and blade chord, the solidity is increased dramatically, which can be detrimental in terms of maximum efficiency. Figure 16 shows the effect of the number of blades but for a case where solidity is maintained constant with the number of blades changing. For comparison, an extra case where $\frac{R}{c}$ is kept the same is also included. Note that in this study, the drag of possible connecting arms is not taken into account.

As expected, increasing the number of blades while keeping the solidity constant does not change significantly the maximum efficiency but it does reduce the fluctuations in the power extracted (Fig. 16). On the other hand, for a turbine with a fixed radius, it is preferable to reduce the number of blades in order to decrease the solidity to achieve better efficiency, although at higher rotational speeds. This is however only valid within a reasonable solidity range. Indeed, a too low solidity would decrease the maximum efficiency, because each blade wake would not be convected fast enough for the next blade to have a clean stream. This reduces the effective angle of attack to the point that no large lift forces are created.

According to the numerical results, the optimal solidity value in the studied conditions, without any alteration to the design (e.g., variable pitch angle), is around $\sigma \approx 0.2$.

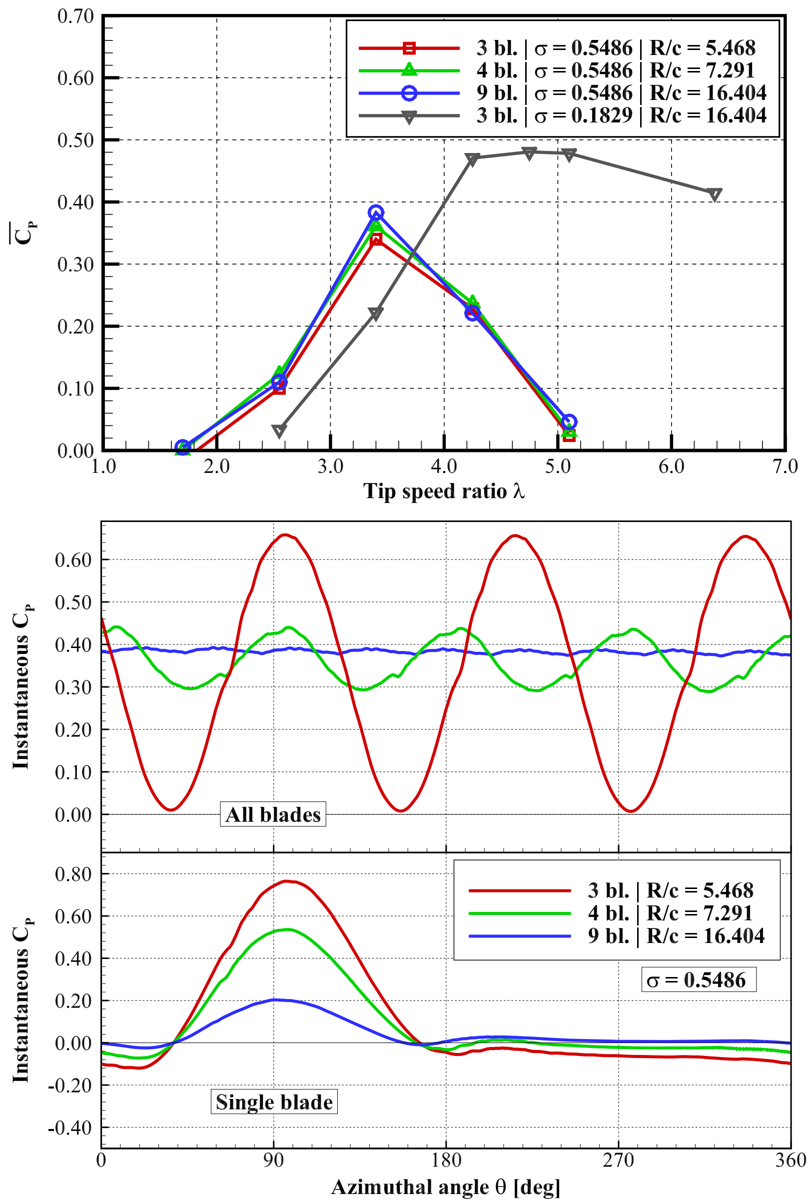

FIG. 16. Effect of the number of blades on the mean and instantaneous C_P in turbines with the same solidity $\sigma = 0.5486$ or the same $R/c = 16.404$.

3. Effect of the blade thickness

Different symmetrical NACA profiles have been tested in a three-blade, $\sigma = 0.5486$ configuration: NACA0012, NACA0015, NACA0020 and NACA0025. Results are shown in Fig. 17.

We see that increasing the blade thickness tends to enlarge the range of TSR where the turbine extracts energy with good efficiency. Increasing it too much however, and the added drag becomes too important and the $\overline{C_P}$ values reached start to plummet.

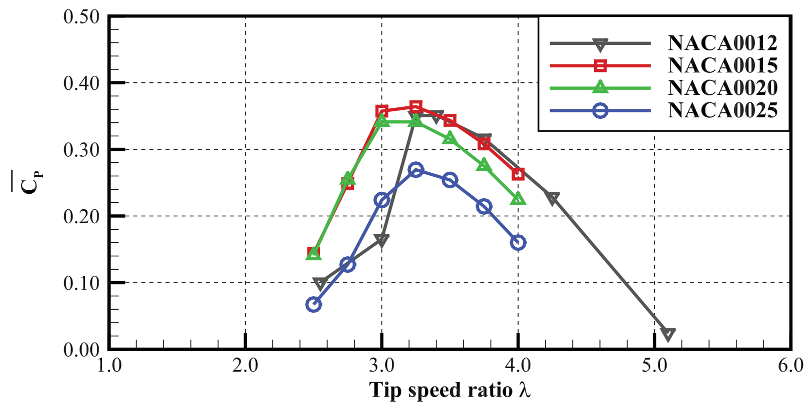

FIG. 17. Effect of the blade thickness in a three-blade turbine with solidity $\sigma = 0.5486$.

In this case, NACA0015 is optimal compared to thinner or thicker profiles. Comparing instantaneous power coefficient at a particularly sensitive TSR ($\lambda = 3$, close to the rotational speed of peak efficiency) for one of the three blades helps understand the differences between each of these cases (Fig. 18).

On the first part of the cycle, before 90°, NACA0012 is slightly better than the other thicknesses, due to its lower drag. However, the sharp decline in power coefficient around 100° observed with NACA0012 is the result of the blade stalling. The thicker profiles does not exhibit stall in these operating conditions, allowing them to reach a higher mean $\overline{C_P}$ value overall.

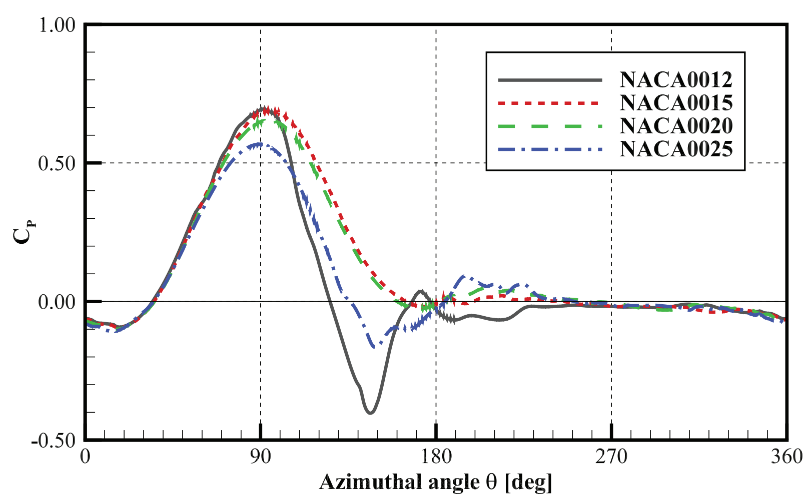

FIG. 18. Instantaneous power coefficient of one of the blades in a three-blade turbine with solidity $\sigma = 0.5486$ at $\lambda = 3.0$.

4. *Effect of a fixed pitch angle*

Various experiments showed that, at least for high solidity cases, changing the pitch angle from $\alpha_0 = 0°$ to a small toe-out angle increases the efficiency of the turbine[11,12]. Simulations with non-zero pitch angle α_0 (see Fig. 3) have been performed for a three-blade turbine with $\sigma = 0.5486$, and global results are shown in Fig. 19.

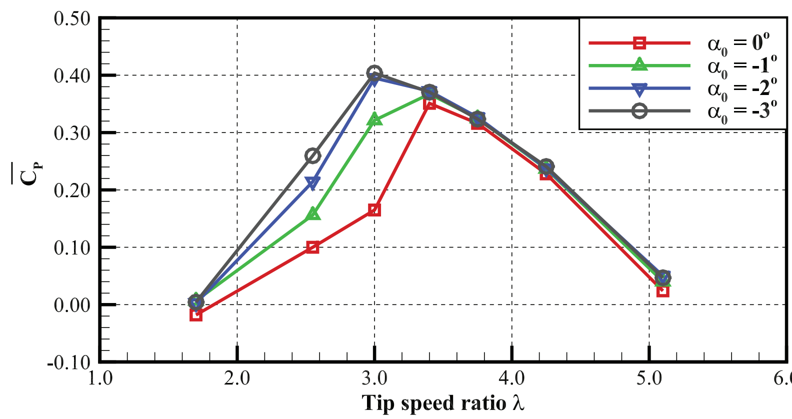

FIG. 19. Effect of the pitch angle α_0 on the efficiency of a three-blade turbine with solidity $\sigma = 0.5486$.

The case at $\lambda = 3.0$ is the best example to help understand in which way setting a small toe-out angle improves the efficiency of the turbine. A comparison of the corresponding instantaneous power coefficients is presented in Fig. 20.

Setting a small amount of toe-out angle on the blade has the effect of reducing the angle of attack in the upstream phase, and increasing it in the downstream one. Both these effects are good for a Darrieus turbine, as the angles of attack are too high in the first pass due to the free stream velocity, and too low (in negative values) in the second phase due to the velocity deficit.

It is clearly visible on Fig. 20 that increasing the negative pitch angle delays power extraction as the actual angle of attack is lower. It also permits to avoid the stall that is present in the $\alpha_0 = 0°$ and $\alpha_0 = -1°$ cases. Finally, the power extracted in the downstream phase is slightly higher with the largest negative pitch angle $\alpha_0 = -3°$, because this turbine extracts a little bit less energy in the upstream phase.

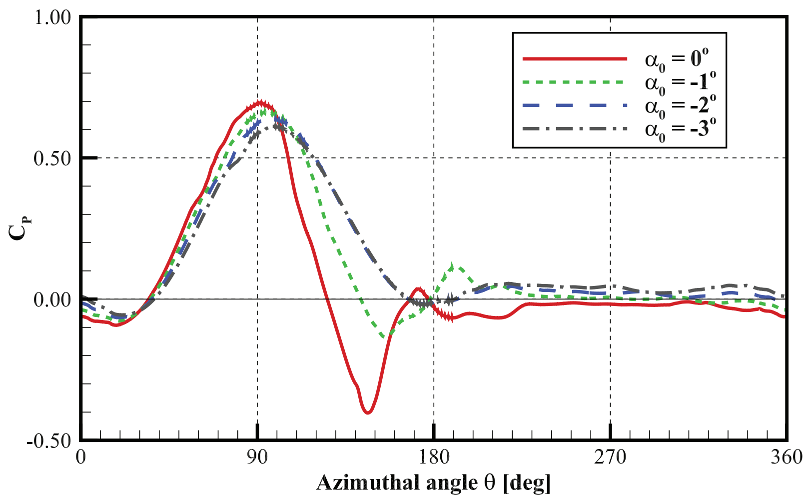

FIG. 20. Instantaneous power coefficient of one of the blades of a three-blade turbine with solidity $\sigma = 0.5486$ at $\lambda = 3.0$, for various pitch angle values.

5. Effect of the Reynolds number

The Reynolds number has a significant effect on the aerodynamics of a wing profile in general. Larger values help delay stall and lower the drag thanks to the boundary layer being more resistant to separation. It also allows slightly higher lift coefficients while reducing slightly the drag coefficient due to the slender effective bodies of the blades.

On the simulation point of view, the only difference is that the boundary layer is thinner in a high Reynolds number case than it is in a low one, so the mesh close to the blade has to be adapted in order to keep the y^+ value below 1. This leads to denser meshes, hence longer calculations. For comparison purposes, single-blade turbine have thus been used here in order to keep the calculation cost low for this particular analysis.

Simulations of a single-blade, $\sigma = 0.1829$ turbine have been carried out with two different Reynolds numbers. The high-Reynolds turbine operates at $Re = 1.5 \times 10^6$ and $\lambda = 5.1$, while the low-Reynolds turbine operates at $Re = 3 \times 10^5$ and $\lambda = 5.1$, the same as the Sandia turbine[2]. Other simulations of the same turbines have been run at a lower TSR, $\lambda = 3.4$, in order to evaluate the effect of increasing the Reynolds number in stalled cases. Results are summarized in Table II, and the instantaneous power coefficients are compared in Fig. 21.

At $\lambda = 5.1$, close to the peak efficiency, the difference between low Reynolds and high Reynolds number cases appears only in the upstream phase, where the power coefficient of the high-Re case

TABLE II. Numerical comparison of the effect of Reynolds number at low and high TSR.

	$\lambda = 3.4$		$\lambda = 5.1$	
Re	2×10^5	1×10^6	3×10^5	1.5×10^6
$\overline{C_P}$	0.158	0.474	0.454	0.508
Relative difference	66.7%		10.6%	

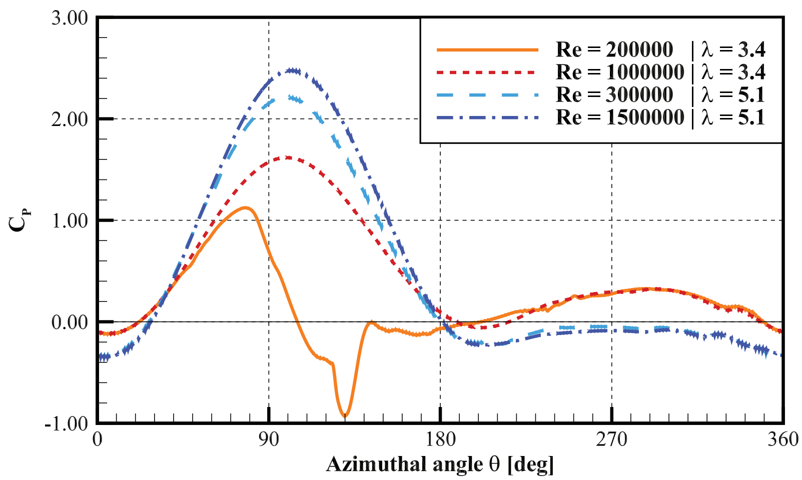

FIG. 21. Comparison of instantaneous power coefficient of a single-blade turbine with solidity $\sigma = 0.1829$ at $\lambda = 3.4$ and $\lambda = 5.1$, for various Reynolds numbers.

reaches a slightly higher value, due to the higher lift and lower drag. There is almost no differences in the downstream phase, where the effective local Reynolds numbers are lower and relatively closer between the two simulations.

At $\lambda = 3.4$, differences are much more important, mainly due to the fact that for the high-Reynolds case, the blade does not stall thanks to a stronger boundary layer, which is not the case in the low-Reynolds case.

Previous studies, e.g.[12], suggest that there is more or less a Reynolds number independence over $Re = 5 \times 10^5$ in the case of Darrieus turbines. In most practical applications, the Reynolds number would typically be higher than this value.

C. 3D effects

In this part of the study, a simple single-blade NACA0015 turbine has been used, with blade aspect ratios of $AR = H/c = 7$ and $AR = 15$. Two different end-plates have also been tested in the

$AR = 7$ case. The turbine solidity is $\sigma = 0.2857$, and simulations are carried out at $\lambda = 4.25$ and $Re = 2.5 \times 10^5$, slightly past the maximum efficiency tip speed ratio, in order to avoid massive stall that would require a much finer mesh and time step size, as discussed in section II C.

A simulation is also presented on a full three-blade turbine with blade aspect ratio $AR = 7$ and solidity $\sigma = 0.5486$ at TSR $\lambda = 3.4$ (peak efficiency), in order to confirm the differences observed on the single-blade turbines.

All those results are compared below to their 2D equivalents.

1. *Blade aspect ratio effect*

Table III shows the results obtained for the two aspect ratios tested. Figure 22 shows the contribution of each 10^{th} of half-blade to the overall energy extraction, depending on its position along the blade span.

TABLE III. Numerical comparison between the performance of 3D turbines with different blade aspect ratios, and the 2D results for a single blade turbine with $\sigma = 0.2857$ at TSR $\lambda = 4.25$. Results for a three-blade turbine with solidity $\sigma = 0.5486$ at TSR $\lambda = 3.4$ are also provided.

Turbine	Number of blades	$\overline{C_P}$	3D/2D performance ratio
2D	1	0.38	–
$AR = 7$	1	0.16	41.8%
$AR = 15$	1	0.26	69.0%
2D	3	0.35	–
$AR = 7$	3	0.19	53.7%

Previous experimental studies[14] have shown that a turbine performance is heavily linked to its blades aspect ratio, with 95% of the 2D efficiency value obtained with $AR > 72$. As modelling such turbines requires a very large domain and a large mesh and, would thus be too computationally expensive, the present comparisons have been made with lower blade aspect ratios.

As expected, the drop is massive with the $AR = 7$ blade, where only 41.8% of the 2D efficiency is reached. Doubling the aspect ratio gives a significant boost in efficiency, reaching nearly 70% of the ideal 2D case. This tendency is in agreement with Li et al. results[14].

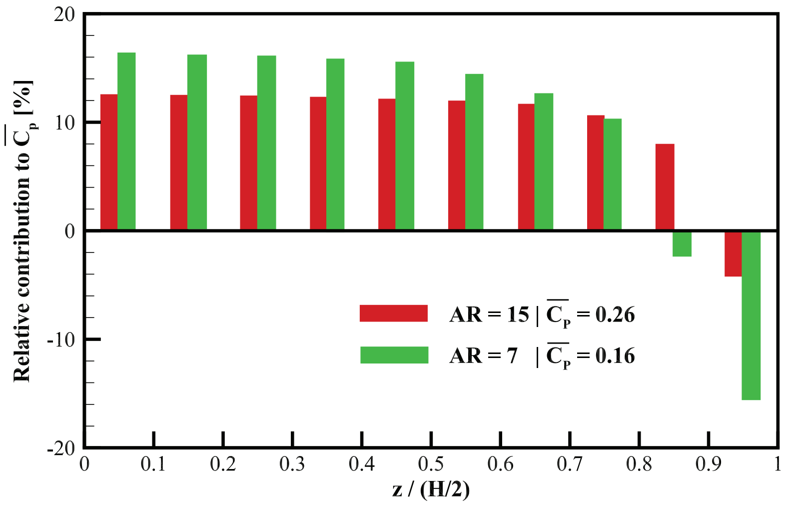

FIG. 22. Comparison of the local contribution to $\overline{C_P}$ along the half-blade span for the $AR = 7$ and $AR = 15$ cases.

It is also noteworthy that the $AR = 7$ simulation of the three-blade turbine gives an efficiency drop smaller than the one observed in the single-blade case. This is an interesting by-product of increasing the number of blades (the main objective being smoothing the torque output), which means that the extraction efficiency is more evenly divided between the blades. On one hand, this means that each blade performance is worse than in a turbine with fewer blades, especially in the upstream part of the cycle, where the maximum C_P reached is lower. On the other hand, this decrease in individual performance is beneficial when considering 3D effects and the drop due to the blade aspect ratio, which is directly linked to the instantaneous lift coefficient. The higher the lift on a blade, the higher the induced drag associated to the finite-span effect. Thus, with the same blade aspect ratio, a turbine with similar overall 2D efficiency but an increased number of blades will perform better thanks to a lower induced drag on the blades. Still, a near 50% drop in performance with regard to 2D results is massive, and improvements are required on that aspect.

The effect of lengthening the blade is illustrated in Fig. 22 from the contribution of each 10^{th} of a half-blade span to total $\overline{C_P}$. The contribution of each blade section is more uniform in the case of the longer blade (a perfect distribution would be 10% for each 10^{th} of the half-blade span), meaning that the flow has a more 2D behaviour when using a longer blade. As expected, the presence of the blade tip is relatively less detrimental with a longer blade.

Fig. 23 shows a visualization of the difference between the center part of the blades and the wingtips. Extraction performance is heavily linked to the axial velocity downstream of the upstream blade, as discussed in section III A 1. One can infer the convection difference along the blade span, with the wingtip vortices being convected about twice as much as the wakes in the center plane.

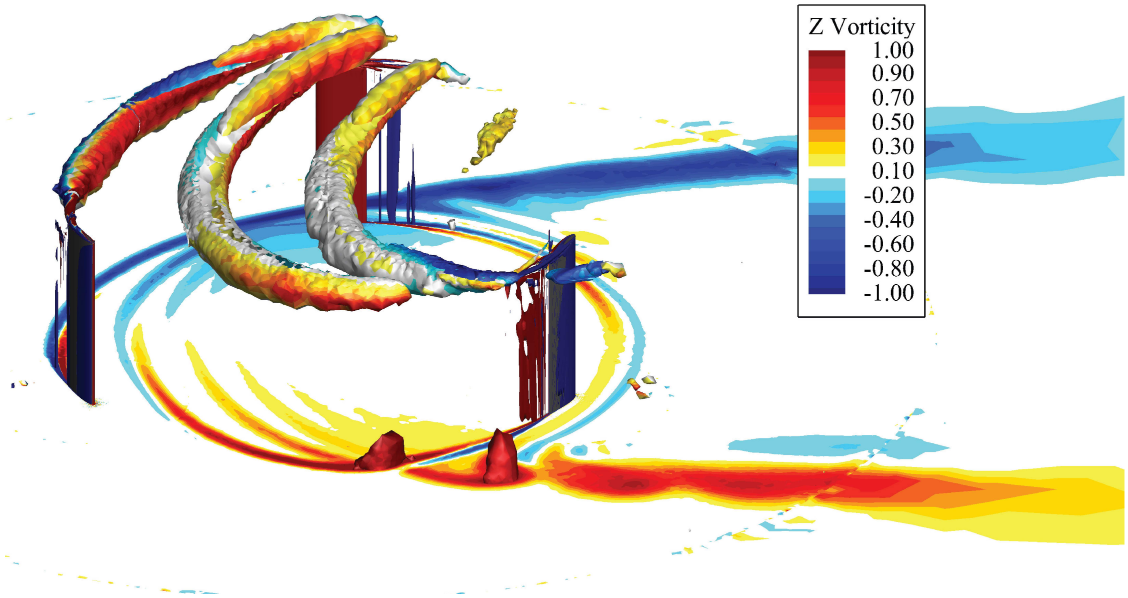

FIG. 23. Isosurface of $\lambda_2 = -0.15$ criterion and contours of Z vorticity on the center plane of a three-blade turbine, $AR = 7$, $\sigma = 0.5486$, TSR $\lambda = 3.4$.

2. End-plates effect

Two types of end-plates have been simulated in order to evaluate the gain in performance made possible by preventing formation of blade-tip vortices. Figure 24 shows the various configurations tested and their effect on the pressure at the blades.

The first one consists in a circular flat plate with no thickness, covering the whole blade mesh area (diameter $= 4c$). The second one is a $0.15c$ extension of the blade profile, which we refer to as the "NACA" end-plate. Figure 25 (similar to Fig. 22) and Table IV compare these results with those of the 2D and the no-end-plate simulations.

While they help reduce the blade tip effect, end-plates have a significant area exposed to the flow, and create additional friction drag that results in a resistive torque on the turbine axis, lowering its efficiency. This cost in efficiency is computed for each case, and is presented in Table IV.

The simulation with the large circular end-plate is interesting in two aspects. The first one is that it shows that it is possible to have an almost constant load distribution on the blade, closer to the 2D optimum case (see Fig. 25). The second point is that the Darrieus turbine is very sensitive to drag, and the benefit of uniform loading is completely annihilated by the energy loss associated to the drag of this large flat plate.

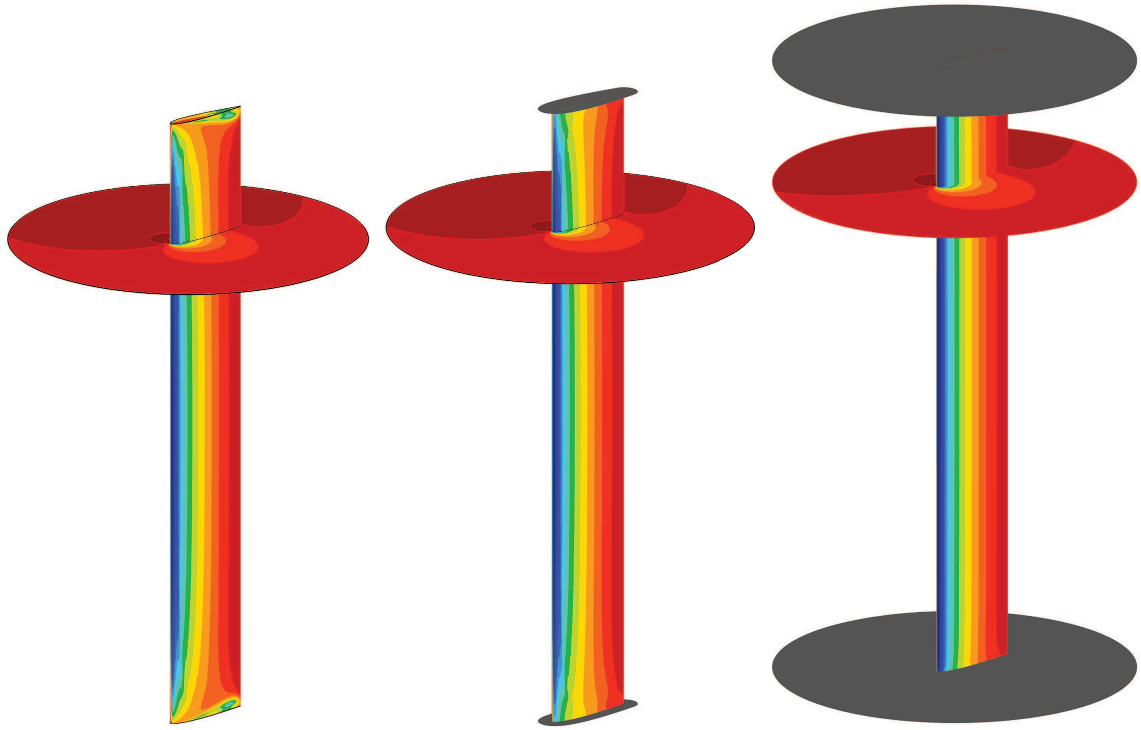

a. No end-plate. b. NACA end-plate. c. Circular end-plate.

FIG. 24. Contours of pressure on the blade at $\theta = 108°$, close to the peak instantaneous C_P, for the three $AR = 7$ configurations.

TABLE IV. Numerical comparison between the performance of 3D turbines with different end-plates, and the 2D results.

Turbine	End-plate	Total $\overline{C_P}$	3D/2D performance ratio	End-plate $\overline{C_P}$ cost
2D	–	0.378	–	–
$AR = 7$	none	0.158	41.8%	–
$AR = 7$	circular	−0.105	–	0.409
$AR = 7$	"NACA"	0.188	49.7%	0.017

The NACA end-plate offers slightly less effective spanwise uniformization, but it offers a 10% efficiency boost compared to the case with no end-plate, which is quite interesting for such a small end-plate. Most of the improvement is made in the region close to the blade tip (compare Fig. 22 and 25). It shows that a small end-plate device can be quite useful in situations where the blade aspect ratio is limited, but the design/size of this end-plate is critical, and a badly sized one may cost a lot more energy than the gain it offers.

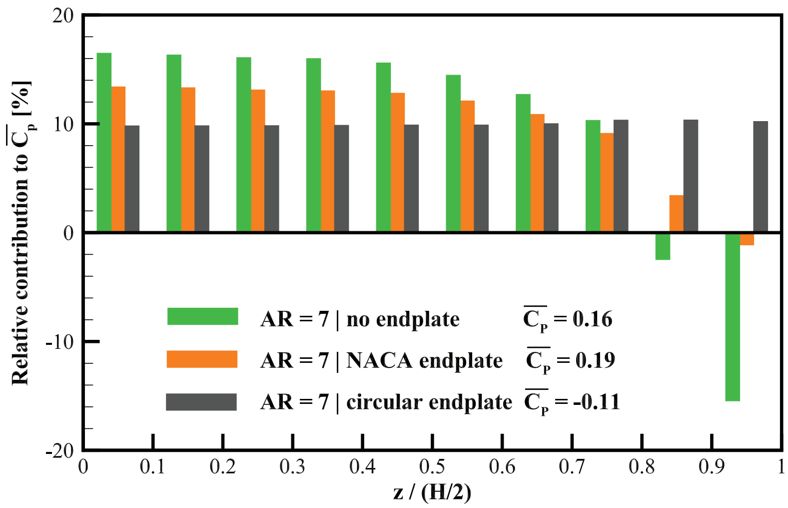

FIG. 25. Comparison of the local contribution to $\overline{C_P}$ along the half-blade span for the $AR = 7$ case with and without end-plates.

IV. CONCLUSIONS

This parametric study of fixed-blades turbines shows that the best performing turbines have solidities around $\sigma = 0.2$, implying turbines with large radius-to-chord ratios. Most real-size Darrieus turbines in the 70s had 2 blades, which produced the best efficiency with reasonable turbine radii. However, torque ripples in such turbines were so important that their mechanical components always failed in the long term, a significant drawback compared to their HAWT counterparts. Nowadays, prototypes with three blades (or more) are more common. They have much less torque ripples but an increased solidity that tends to reduce their maximum efficiency. The simulations presented here confirm the experimental observations that turbines with solidities around $\sigma = 0.5$ display a lower efficiency than ones with lower solidities, contrary to published simulation results in the 80s. This shows that earlier model are not very efficient in this range of tip speed ratio and tend to overestimate the efficiency value.

On a design standpoint, expecting great efficiencies "out of the box" for high solidity turbines is not realistic. However, simulation results for fixed, non-zero, pitch angle cases show that there is a great potential of improvement in medium tip speed ratios (2 to 4) for turbines with solidity around 0.5. For example, a small pitch angle adjustment radically changes the efficiency at low tip speed ratios, by delaying stall. There is also a large sensitivity to the profile thickness, showing the critical effect of stall behaviour in this particular operating range. These observations open the way to dynamic pitch control, with the ability to maximize blade lift to drag ratio over a complete cycle.

The preliminary results from 3D simulations show that high blade aspect ratio $AR = H/c$ is necessary in order to reduce the drop of efficiency between ideal 2D turbines and real ones. End-plates may help limiting 3D losses but their size should be minimized in order to limit the added drag.

Further studies using the proposed of simulation methodology are needed in order to optimize the efficiency of a Darrieus turbine. More 3D simulations are essential in order to evaluate precisely the drop between 2D results and an hypothetical real turbine, especially turbines with high blade aspect ratios. Dynamic pitch control functions could also help improve other aspects of a vertical axis turbine, such as self-starting or lower torque ripples[30–32], especially in configurations that imply deep stall with fixed blades.

ACKNOWLEDGEMENTS

Most of the present simulations were computed on the supercomputer Colosse at Université Laval, managed by Calcul Québec and Compute Canada. The authors would like to thank Thomas Kinsey for fruitful discussions and his help with reviewing this manuscript. Financial support from NSERC/DG program is also gratefully acknowledged.

REFERENCES

[1]G. J. M. Darrieus, "Turbine having its rotating shaft transverse to the flow of the current," Patent, http://www.google.com/patents/US1835018 (1926), filed: 1926-10-01, Patented: 1931-12-08.

[2]R. Sheldahl, P. Klimas, and L. Feltz, "Aerodynamic performance of a 5-meter-diameter Darrieus turbine," AIAA Journal of Energy **4** (1980).

[3]K. Pope, I. Dincer, and G. F. Naterer, "Energy and exergy efficiency comparison of horizontal and vertical axis wind turbines," Renewable Energy **35**, 2102–2113 (2010).

[4]J. Templin, "Aerodynamic performance theory for the NRC vertical axis wind turbine," Tech. Rep. (NRC Institute for Aerospace Research; National Research Council Canada, 1974).

[5]J. Strickland, "The Darrieus turbine: a performance prediction model using multiple streamtubes," Tech. Rep. (Sandia Laboratories, 1975).

[6]I. Mays and B. A. Holmes, "Commercial development of the variable geometry vertical axis windmill," International Power Generation, Surrey, UK (1979).

[7]W. Grylls, B. Dale, and P. Sarre, "A theoretical and experimental investigation into the variable pitch vertical axis wind turbine," Proc. 2nd Int. Symposium on Wind Energy Systems **E9**, 101–118 (1978).

[8]E. Williams Beans, "Approximate aerodynamic analysis for multi-blade Darrieus wind turbine," Journal of wind engineering and industrial aerodynamics **25**, 131–150 (1987).

[9]I. Paraschivoiu, *Wind Turbine Design with emphasis on Darrieus concept* (Polytechnic International Press, 2002).

[10]R. Howell, N. Qin, J. Edwards, and N. Durrani, "Wind tunnel and numerical study of a small vertical axis wind turbine," Renewable Energy **33**, 412–422 (2010).

[11]R. Gosselin, *Control of flow separation on Vertical Axis Wind Turbine blades*, Master's thesis, Departement of Mechanical Engineering, University of Sheffield (2008).

[12]S. Armstrong, A. Fiedler, and S. Tullis, "Flow separation on a high Reynolds number, high solidity vertical axis wind turbine with straight and canted blades and canted blades with fences," Renewable Energy **41**, 13–22 (2012).

[13]Mavi Innovations Inc., `http://http://mavi-innovations.ca/` (2014), accessed: 2014-11-09.

[14]Y. Li and S. Calisal, "Three-dimensional effects and arm effects on modeling a vertical axis tidal current turbine," Renewable Energy **35**, 1–10 (2010).

[15]S. Ferreira, H. Bijl, G. van Bussel, and G. van Kuik, "Simulating dynamic stall in a 2d VAWT: Modeling strategy, verification and validation with particle image velocimetry data," Journal of Physics **Conference Series 75** (2007).

[16]M. Castelli, A. Englaro, and E. Benini, "The Darrieus wind turbine: Proposal for a new performance prediction model based on CFD," Energy **36**, 4919–4934 (2011).

[17]M. Marini, A. Massardo, and A. Satta, "Performances of vertical axis wind turbines with different shapes," Journal of wind engineering and industrial aerodynamics **39**, 83–93 (1992).

[18]G. Rawlings, *Parametric characterization of an experimental vertical axis hydro turbine*, Master's thesis, University of British Columbia (2008).

[19]W. Tjiu, T. Marnoto, S. Mat, M. H. Ruslan, and K. Sopian, "Darrieus vertical axis wind turbine for power generation I: Assessment of Darrieus VAWT configurations," Renewable Energy **75**, 50–67 (2015).

[20]W. Tjiu, T. Marnoto, S. Mat, M. H. Ruslan, and K. Sopian, "Darrieus vertical axis wind turbine for power generation II: Challenges in HAWT and the opportunity of multi-megawatt Darrieus VAWT development," Renewable Energy **75**, 560–571 (2015).

[21]Y. Li, N. Karri, and Q. Wang, "Three-dimensional numerical analysis on blade response of vertical-axis tidal current turbine under operational conditions," Journal of Renewable and Sustainable Energy **6** (2014).

[22]ANSYS Inc., "FLUENT® 14.5 user's guide," (2013), `www.ansys.com`.

[23]S. Wang, D. Ingham, L. Ma, M. Pourkashanian, and Z. Tao, "Numerical investigations on dynamic stall of low Reynolds number flows around oscillating airfoils," Computers & fluids **39**, 1529–1541 (2010).

[24]J. Dacles-Mariani, G. Zilliac, J. Chow, and P. Bradshaw, "Numerical/experimental study of a wingtip vortex in the near field," AIAA Journal **33**, 1561–1568 (1995).

[25]J. Dacles-Mariani, D. Kwak, and G. Zilliac, "On numerical errors and turbulence modeling in tip vortex flow prediction," International Journal for Numerical Methods in Fluids **30**, 65–82 (1999).

[26]S. Zadeh, M. Komeili, and M. Paraschivoiu, "Mesh convergence study for 2-d straight-blade vertical axis wind turbine simulations and estimation for 3-d simulations," Transactions of the Canadian Society for Mechanical Engineering **38**, 487–504 (2014).

[27]C. Devaud, J. Weisinger, D. Johnson, and E. Weckman, "Experimental and numerical characterization of the flowfield in the large-scale UW live fire research facility," International Journal for Numerical Methods in Fluids **60**, 539–564 (2009).

[28]R. Gosselin, *Analysis and optimization of Vertical Axis Turbines*, Ph.D. thesis, Faculté des Sciences et de Génie, Université Laval, Québec (2015), http://www.theses.ulaval.ca/2015/32024/.

[29]B. K. Kirke, *Evaluation of self-starting vertical axis wind turbines for stand-alone applications*, Ph.D. thesis, School of Engineering, Griffith University, Gold Coast Campus (1998).

[30]I. Paraschivoiu, O. Trifu, and F. Saeed, "H-Darrieus wind turbine with blade pitch control," International Journal of Rotating Machinery **Volume 2009** (2009).

[31]B. Kirke and L. Lazauskas, "Experimental verification of a mathematical model for predicting the performance of a self-acting variable pitch vertical axis wind turbine," Wind engineering **17**, 58–66 (1993).

[32]S. Sarkar and K. Venkatraman, "Influence of pitching angle of incidence on the dynamic stall behavior of a symmetric airfoil," European Journal of Mechanics B/Fluids **27**, 219–238 (2008).